Synthetic Metals 220 (2016) 1–7

Contents lists available at ScienceDirect

Synthetic Metals

journal homepage: www.elsevier.com/locate/synmet

Influences of annealing temperature and thickness on ZnS buffer layers for inverted hybrid solar cells

Fatih Ongul*, Unzile Ulutas, Sureyya Aydin Yuksel, S. Serkis Yesilkaya, Serap Gunes

Yildiz Technical University, Faculty of Arts and Science, Department of Physics, Davutpasa Campus, 34210, Esenler, Istanbul, Turkey

ARTICLE INFO

Article history:
Received 1 March 2016
Received in revised form 10 May 2016
Accepted 18 May 2016
Available online xxx

Keywords:
ZnS thin film
Spray pyrolysis
Inverted structure
Organic solar cells

ABSTRACT

In this study, the photovoltaic performances of inverted type hybrid solar cells fabricated using zinc sulfide (ZnS) as a buffer layer and blend of P3HT(poly(3-hexyl)thiophene), PCBM([6,6]-phenylC61 butyric acidmethylester) as a photoactive layer were reported. ZnS thin films were prepared by spray pyrolysis method at fixed substrate temperature. The effects of annealing under ambient conditions at different temperatures on the optical and structure properties of ZnS films were investigated. When the annealing temperatures of ZnS films were increased from 200 to 500 °C, the power conversion efficiency of the inverted type hybrid solar cells was significantly enhanced by improving crystallite and morphology of buffer layer. The effect of ZnS film thickness on photovoltaic parameters of the inverted devices was also investigated.

© 2016 Elsevier B.V. All rights reserved.

1. Introduction

Solar cells are considered promising devices as a clean source of renewable energy that is an alternative to conventional energy sources for the civil electricity supply. The use of organic semiconductors seen as alternative to inorganic materials is compatible with these purposes. However, organic solar cells suffer from low power conversion efficiencies as compared to the inorganic solar cells. Organic solar cells have some disadvantages such as the poor spectral match with solar emission, the extremely large exciton binding energy, the short diffusion length, and poor stability and degradation; but nevertheless they have gained popularity in recent years due to their multifarious advantages especially such as low cost, lightweight, and flexible and effective large-scale production thanks to being deposited by the solution based techniques. So, new polymeric materials, new combinations and structures have been designed and investigated in organic based solar cells [1–4]. One of the most used concepts in organic photovoltaic is the bulk heterojunction in which the donor polythiophene derivatives such as poly (3-hexylthiophene) (P3HT) and acceptor material fullerene derivative [6,6]-phenyl C61-butyric acid methyl ester (PCBM) are blended together and thereby the interfacial area between donors and acceptors are maximized [5–7].

Organic photovoltaic device architecture associated with the direction of the charge flow is often divided into two groups as normal geometry and inverted geometry. Normal geometry of organic solar cell consists of transparent conductive electrode indium tin oxide (ITO), photoactive layer and a top metal electrode, generally aluminium that degrades rapidly in air because of being instable against oxygen and moisture. In an inverted geometry OPVs, the low work function reactive metal is replaced with more stable one which eliminates oxidation problem, like silver or gold (Ag or Au), while a metal oxide such as TiO_2 and ZnO is introduced in this structure as electron collector layer [8–15]. Organic and inorganic semiconductors are combined in a hybrid solar cell, thus it has the unique properties of inorganic semiconductors as well as having the film forming properties of organic semiconductors. The inorganic materials such as metal oxides, cadmium compounds, ternary compounds, silicon and nanoparticles which have good electronic properties, a high dielectric constant, a high charge mobility and a high light absorption capability have been used as the electron acceptor in the hybrid system for providing these advantages to the photovoltaic system [16]. The hybrid solar cells comprising of ternary absorber layers such as $AgInS_2$, Ag_3CuS_2 and Sb_2S_3 coated on ZnO or ZnO/ZnS core/shell nanotube arrays, and electron donor polymer materials were designed for improving the efficiency of solar cells. The nanoarrays used in the hybrid system provided larger interface area, better charge transport and higher efficiency of light harvesting, which enhanced the efficiency consequently [17–19]. Recently, inverted configuration hybrid solar cells with CdS films as electron transport layer have been

* Corresponding author.
E-mail address: fatihongul@gmail.com (F. Ongul).

http://dx.doi.org/10.1016/j.synthmet.2016.05.017
0379-6779/© 2016 Elsevier B.V. All rights reserved.

fabricated [20,21]. ZnS layer is one of the most promising potential candidate for solar applications due to its no toxicity and wider energy band gap compared to CdS. ZnS is an *n*-type inorganic semiconductor in group II–VI with a direct band-gap and being expected as one of the promising electron transport layer as well as being the hole blocking layer [22,23].

Many deposition techniques as thermal evaporation [24], molecular beam epitaxy [25], chemical vapor deposition [26], chemical bath deposition (CBD) [27] and spray pyrolysis [28] have been used to prepare ZnS thin films. Among them, spray pyrolysis offers number of advantages like low cost source materials, simple deposition equipments and uniform deposition for large area.

In this study, inverted type hybrid solar cells were fabricated with ZnS thin films prepared by the spray pyrolysis method as the electron transport layer and blend of P3HT:PCBM as the photoactive layer in glass/ITO/ZnS/P3HT:PCBM/PEDOT:PSS:IPA/Ag structure (Fig. 1). The optical and structural properties of the ZnS films annealed at different temperatures were examined in detail. The effects of annealing temperature and thicknesses of ZnS films on the efficiency of the devices were investigated.

2. Experimental

Indium tin oxide (ITO) coated glasses with thickness of ca. 120 nm and sheet resistances of 12 ohm/square purchased from Kintec Company were used as substrates. The one-third of ITO with $1.5 \times 1.5\ cm^2$ dimensions had been removed by etching with acid mixture ($HCl:HNO_3:H_2O$) and then substrates were cleaned in an ultrasonic bath with helmanex, distilled water, acetone and isopropanol for 20 min, respectively.

ZnS thin films were deposited on ITO and glass substrates by spray pyrolysis technique using an aqueous solution mixtures of zinc acetate (0.05 M $Zn(O_2CCH_3)_2$) and thiourea (0.0125 M CS $(NH_2)_2$) in distilled water. The precursor solution was sprayed onto substrates, kept at 300 °C for 25 min and solution flow rate was fixed at 2 ml/min. Thereafter, deposition of ZnS thin films was subjected to thermal treatment at different temperatures for 1 h under atmospheric conditions in furnaces. The molar concentrations of zinc acetate and thiourea were reduced four times with the equal molarity amount, and also the volumes of these solutions were decreased twofold for decreasing the thicknesses of ZnS films. The thicknesses of ZnS films were measured by the Veeco Dektak profilometer. The blends of P3HT:PCBM with 1:0.55 wt ratios in 1 ml of chlorobenzene (CB) used as active layer were coated on top of ZnS films under environmental conditions. PEDOT:PSS, Clevios Heraeus Co., poly(3,4-ethylenedioxythiophene): poly(styrene-sulfonate) filtered using a 0.45 μm Whatman filter was diluted with isopropanol in 1:20 vol ratios, spin coated onto the active layer at 800 rpm, 30s, and then annealed at 120 °C for 3 min under atmospheric conditions in furnaces. Silver (Ag) electrode on top of the films was thermally evaporated in vacuum chamber ($1{\cdot}10^{-5}$mbar) at 5.0 Å/sec with thickness of 100 nm controlled by deposition controller.

FEI-Quanta FEG 250 scanning electron microscopy was used to observe the surface morphologies of the ZnS films. The crystalline structures of ZnS thin films annealed at different temperatures were analysed using X-ray diffraction (XRD, Panalytical Diffractometer Philips) with Cu Kα radiation (λ=1.54056 Å) in the range of 5°–80°. The lattice constants of the ZnS thin films with wurtzite phase structure were calculated from Eq. (1). Debye-Scherrer's Formula given in Eq. (2) was used for estimating the average crystallites of the thin films. The dislocation density (δ) given in Eq. (3) Williamson and Smallman's formula, which is related to the dislocation lines per unit area in the film, was estimated using the average of the grain size (D) [29].

$$\frac{1}{d^2} = \frac{4}{3}\left(\frac{h^2 + hk + k^2}{a^2}\right) + \frac{l^2}{c^2} \quad (1)$$

$$D = K\lambda/(\beta\cos\theta) \quad (2)$$

$$\delta = 1/D^2\ (lines/m^2) \quad (3)$$

Where in the Eq. (1), a and c are the lattice constants, d is the distance between adjacent lattice planes and (hkl) is Miller indices. Where in the Eq. (2), D is the crystal size, K is the constant shape factor (0.9), λ is the wavelength of X-ray radiation source, θ is the diffraction angle and β is the full width at half maximum of the prominent peak in radian.

The transmission spectra of ZnS thin films were carried out using the ultraviolet–visible spectrophotometer (Lambda-2 Perkin–Elmer) in the wavelength range of 320–1000 nm. The energy band gap of ZnS films with direct band gap was calculated using the relation given in Eq. (4) [30];

$$\alpha^2 = B(h\nu - Eg)/(h\nu)^2 \quad (4)$$

Where α is the absorption coefficient, hν is the photon energy, Eg is the energy band gap of film and B is a constant. The extrapolation of the straight line to hν axis at $(\alpha h\nu)^2 = 0$ on the plot of $(\alpha h\nu)^2$ versus hν gives the value of energy band gap (Eg).

Hybrid solar cell was designed in the inverted geometry in the form of ITO/ZnS/P3HT:PCBM/PEDOT:PSS:IPA/Ag, and photovoltaic properties of these structures were investigated depending on the annealing temperature and the thickness of ZnS window materials. Photovoltaic performances of devices were examined using a computer controlled Keithley 2400 sourcemetre in dark and under

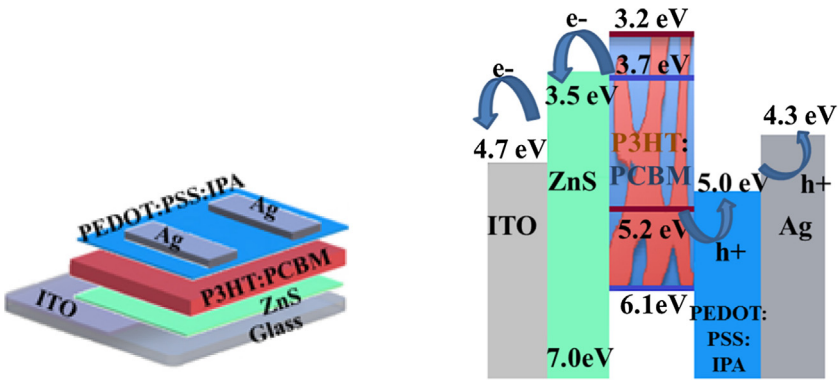


Fig. 1. (a) Schematic device architecture and (b) energy level diagram of the device with glass/ITO/ZnS/P3HT:PCBM/PEDOT:PSS:IPA/Ag structure.

illumination that is provided with AM1.5 G solar simulator (Lutzchem) calibrated by standard crystalline silicon reference diode set at 100 mW/cm^2. Photovoltaic parameters such as short-circuit current density J_{sc} (mA/cm^2), open-circuit voltage V_{oc} (V), fill-factor FF, and parasitic resistances including the series resistance (R_s) and the shunt resistance (R_{sh}) were determined from the current density-voltage (J-V) characteristic. The power conversion efficiency ($\eta_{Am1.5}$) is given by the ratio of power-out to power-in as a percentage (Eq. (5)). Fill factor (FF) is defined as the ratio of convertible maximum power point (mpp) of the solar cell to the product of the maximum power of the ideal solar cell (Eq. (6)).

$$\eta_{AM1.5}(\%) = \left(\frac{P_{out}}{P_{in}}\right) \times 100 = \frac{FF \times V_{oc} \times J_{sc}}{P_{in}} \times 100 \quad (5)$$

$$FF = \frac{V_{mpp} \times J_{mpp}}{V_{oc} \times J_{sc}} \quad (6)$$

The incident photon-to-current conversion efficiency (IPCE) spectra of inverted configuration hybrid solar cells were obtained using New Port Quantum Efficiency Systems. The theoretical short circuit current density (J_{IPCE}) was calculated from the IPCE spectra using the Eq. (7).

$$J_{sc} = \int qF(\lambda)\ IPCE(\lambda)d\lambda \quad (7)$$

Where $F(\lambda)$ is the incident photon flux density at AM 1.5 G condition, $IPCE(\lambda)$ is the spectral responsivity, q is the electron charge and λ is the wavelength of light.

3. Results and discussion

The XRD patterns of the ZnS thin films as deposited and annealed at different temperatures as 200, 300, 400, 500 °C for 1 h are shown in Fig. 2. The ZnS thin films showed hexagonal phase that the diffraction peaks of the films were close to 27.02°, 28.64°, 30.65°, 39.78°, 47.73°, 52.00° and 56.61° for (100), (002), (101), (102), (110), (103) and (112) crystal planes of wurtzite phase, according to AMCSD database code 0015179 [31], and the other relatively small peaks indicated the formation of new phases $ZnSO_4$ and ZnO because of incorporation of oxygen atoms in the ZnS films. These small peaks were compatible with (101), (111) and (301) plane of $ZnSO_4$ at 21.28°, 25.09° and 36.55°, and (100), (002) and (101) plane of ZnO at 31.80°, 34.47° and 36.29° corresponding to AMCSD database code 0014620 and 0005205, respectively [32,33]. It was reported by several authors that the peak positions for the wurtzite or sphalerite phases of ZnS thin films shifted from the typical positions. This difference may be proceeding from the lattice expansion or distortion due to the new phases of impurities

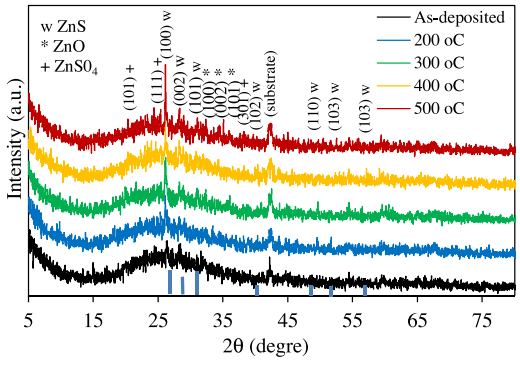


Fig. 2. XRD patterns of ZnS thin films as deposited and annealed at 200–500 °C for 1 h.

or intrinsic defects such as vacancies and interstitials [34–39]. It was shown in Fig. 2 that as annealing temperature was increased, the peak intensity at oriented along (100) direction also increased corresponding to improvement of crystallinity. The lattice constants, crystallite sizes and dislocation densities of ZnS thin films annealed at different temperatures were calculated from XRD data and are illustrated in Table 1. It was observed that the crystallite size of ZnS thin films increased from 27 to 153 nm when the annealing temperature increased from 200 to 500 °C accompanied by an improvement in crystal structure with annealing. The dislocation density values (δ) of ZnS thin films calculated from grain sizes were decreased from 13.7 10^{14} to 0.43 10^{14} (lines/m^2) with increasing temperature of annealing from 200 to 500 °C. The reduction dislocation density indicated the decrease of the number of grain boundary in ZnS thin film.

The intensity of optical transmission of ZnS thin films increased with increasing annealing temperature due to improved crystallinity of the ZnS thin films as shown in Fig. 3a. The optical band-gap values of ZnS thin films with direct transition were determined from Tauc plot of $(\alpha h\nu)^2$ versus photon energy $h\nu$ as shown in Fig. 3b. The band gap energy (E_g) was determined from the intercept of the extrapolated linear part of the curve to zero absorption with the photon energy axis. The optical band gap values for ZnS thin films varied between 3.30 eV and 3.55 eV depending on annealing temperature. At first, optical band-gap of ZnS films increased from 3.35 eV to 3.55 eV with increasing annealing temperature up to 400 °C and then the optical band-gap decreased to 3.30 eV at 500 °C as shown in Table 1.

Scanning Electron Microscope (SEM) was used for investigating the surface morphologies of the ZnS thin films. SEM images of ZnS thin films as deposited and annealed at 500 °C for 1 h are shown in Fig. 4. As can be seen from the images, ZnS thin film that was exposed to thermal annealing at 500 °C for 1 h exhibited rather homogeneous and smooth surface morphology as compared to ZnS thin film as deposited. SEM images and X-ray diffraction patterns indicated that as-deposited ZnS films were partially amorphous, and thermal treatments improved the structure and surface morphology.

The photovoltaic performances of the inverted devices fabricated with and without ZnS as an electron transport layer that was exposed to annealing at different temperatures were investigated. The current density-voltage characteristics of these devices under illumination on a single figure are illustrated in Fig. 5. The photovoltaic parameters of these devices such as V_{oc}, J_{sc}, FF, PCE, and parasitic resistances such as the series resistance (R_s) and the shunt resistance (R_{sh}) determined from the current density-voltage curves are illustrated in Table 1. As a reference cell, the device without ZnS interlayer as an electron transport layer showed low photovoltaic performance. After using as deposited ZnS thin film, electron-transporting layer with hole-blocking properties, and photovoltaic performances of the device as open circuit voltage and fill factor increased, whereas short circuit current density and power conversion efficiency decreased, as compared to the reference device. The unannealed ZnS thin film with high resistance (2.21 10^{11} Ω/sq), partially amorphous structure and also rough surface morphology led to low photocurrents in this inverted device. Furthermore, as the annealing temperatures for ZnS thin films were increased from 200 to 500 °C, the efficiencies of the devices significantly increased up to 0.254% with increase of J_{sc} from 0.018 to 2.33 mA/cm^2 and also V_{oc} from 0.23 to 0.41 V. The series resistances and the shunt resistances of devices decreased significantly with increasing temperature of annealing. It was determined that the crystallinity and the particle size of ZnS thin films were influenced by the annealing temperature. The improvement of crystallinity and the increase in particle size thanks to increasing temperature of annealing

Table 1
Properties of ZnS films and the photovoltaic parameters of inverted devices with and without ZnS thin films as deposited and annealed at different temperatures.

	Without ZnS	As Deposited	Annealed200 °C	Annealed 300 °C	Annealed 400 °C	Annealed 500 °C
ZnS-E_g (eV)		3.35	3.35	3.5	3.55	3.30
ZnS-a (nm)		–	3.91	3.93	3.94	3.94
ZnS-c (nm)		–	6.39	6.42	6.44	6.44
ZnS-D (nm)		–	27	52	76	153
ZnS δ (10^{14} lines/m^2)		–	13.7	3.70	1.73	0.43
V_{oc} (mV)	100	230	250	250	270	410
J_{sc} (mA/cm^2)	0.35	0.018	0.04	0.22	0.58	2.33
FF	0.19	0.26	0.23	0.26	0.25	0.27
PCE (%)	0.007	0.001	0.002	0.014	0.039	0.254
R_s (kΩcm^2)	0.204	11.35	6.552	1.153	0.444	0.168
R_{sh} (kΩcm^2)	0.192	17.381	6.163	1.070	0.472	0.204

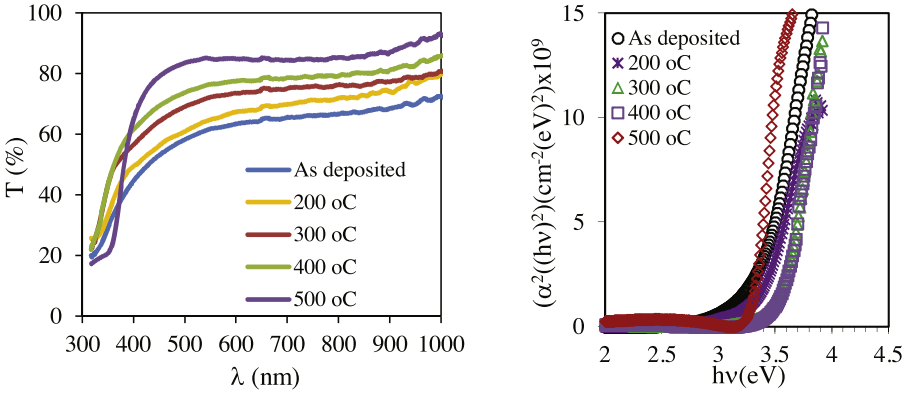


Fig. 3. The optical transmission spectra (a) and the absorption spectra (b) of the ZnS films with as deposited and annealed at 200, 300 400 and 500 °C for 1 h.

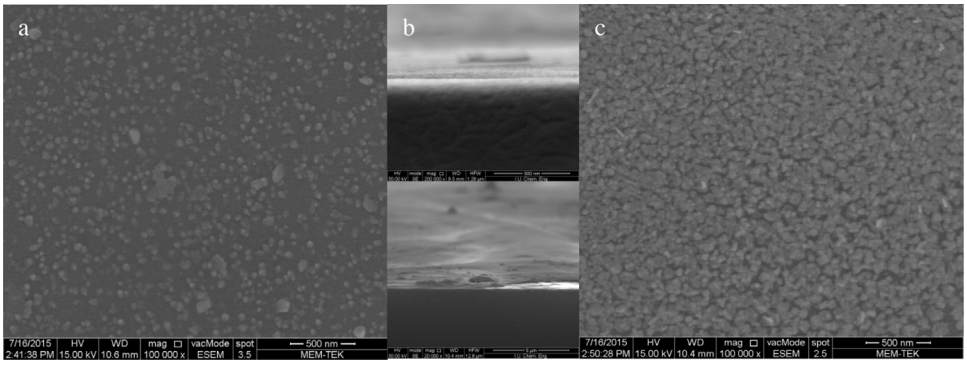


Fig. 4. (a) Top view and (b) side view SEM images of the as-deposited ZnS thin film and (c) top view SEM image of the ZnS thin film annealed at 500 °C for 1 h.

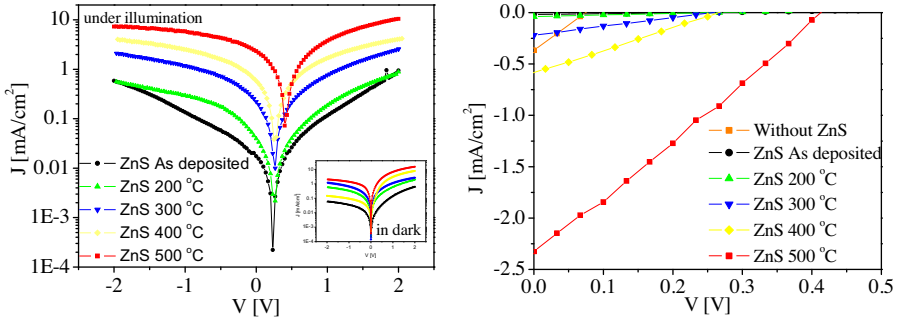


Fig. 5. Current density-voltage characteristics of the inverted devices with and without ZnS interlayer as deposited and annealed at different temperatures, in dark and under simulated AM1.5 G illumination at 100 mW/cm^2.

provided the reduction of defects and the decrease grain boundary, which led to enhance the charge transport and charge collection efficiency, and resulted in increment of J_{sc} and V_{oc} in devices [40]. The ZnS thin film annealed at 500 °C for 1 h with low resistance of 3.79 10^7 Ω/sq, high crystallinity structure, high optical transmission and also smooth surface morphology led to the higher efficiency as compared to devices employing unannealed ZnS films. Highly crystalline ZnS films upon annealing are off important to achieve a higher efficiency. Enhancement in the photovoltaic performances of inverted devices may be attributed to improved crystalline structure and a smooth morphology of ZnS interlayer which in turn may affect the transport properties.

ZnS interlayers with different thicknesses varying from 135 to 476 nm were deposited on ITO by adjusting the molar concentration of the precursor solution. The influences of thickness of ZnS electron transport layers annealed at 500 °C for 1 h on the performances of inverted devices were also investigated. Fig. 6 shows the current density–voltage characteristics of the inverted type organic solar cells prepared with ZnS thin films with thickness of 476, 322, 243 and 135 nm. Photovoltaic parameters of these devices were determined from Fig. 6 and are displayed in Table 2. As can be seen from Table 2 and Fig. 6, the power conversion efficiencies of these inverted devices increased with increase of the short circuit current density and the open circuit voltage, and decrease of the thickness of ZnS interlayer. The series resistance (R_s) and the shunt resistance (R_{sh}) of the inverted devices reduced slightly with decreasing thickness of ZnS thin films. The highest photovoltaic parameters as J_{sc} of 3.45 mA/cm^2, V_{oc} of 0.49 V, FF of 0.27 and PCE of 0.45% were achieved for inverted organic solar cells employing 135 nm thick ZnS thin films.

The decreased transmittance with increased thickness of ZnS interlayer may be related to surface roughness as the consequence of formation of uncontrolled cluster or agglomeration during deposition of the layer. The surface morphology of the film may change with increasing film thickness, so smooth thin films are more suitable for being used as interlayer in organic solar cells [20]. The properties of the interface between organic and inorganic layers play an important role; therefore the first inorganic layer is desired to have good quality, good homogeneity, smooth surface, high transmittance and good electrical properties. The results indicate that the efficiency of inverted devices can be significantly influenced by the thickness of ZnS interlayer. As shown in Fig. 7, optical transmittance of ZnS thin layer increased specially in the range of 300–650 nm as decreasing thickness of ZnS interlayer because the first layer that light passes through plays an important role in the inverted devices performance.

The incident photon-to-current conversion efficiency (IPCE) is defined as the ratio of the number of collected charges in the external circuit photogenerated by an incident monochromatic light at a given wavelength. IPCE spectrum provides information for solar cells in which portion of solar spectrum light harvesting. The IPCE spectra of the inverted devices with different ZnS thicknesses are shown in Fig. 8 and also the J_{sc} values of these devices calculated using the IPCE values are illustrated in Table 2.

Table 2
Photovoltaic parameters of inverted devices employing ZnS layer with different thicknesses.

	A ZnS 476 nm	B ZnS 322 nm	C ZnS 243 nm	D ZnS 135 nm
V_{oc} (mV)	410	430	450	490
J_{sc} (mA/cm^2)	2.43	2.93	3.19	3.45
FF	0.27	0.26	0.26	0.27
PCE (%)	0.27	0.33	0.38	0.45
J_{IPCE} (mA/cm^2)	2.14	2.67	2.93	3.23
R_s (kΩcm^2)	0.149	0.142	0.131	0.130
R_{sh} (kΩcm^2)	0.204	0.163	0.160	0.158

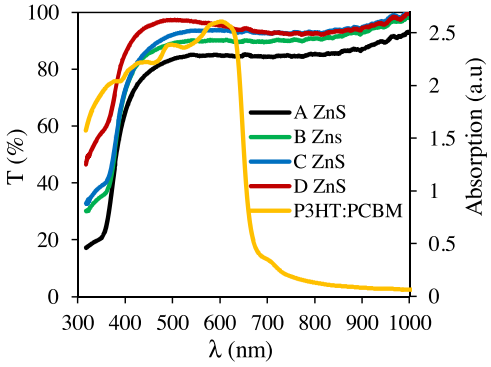


Fig. 7. The optical transmission spectra of ZnS films with different thicknesses (A, B, C and D) and the absorption spectra of the P3HT:PCBM.

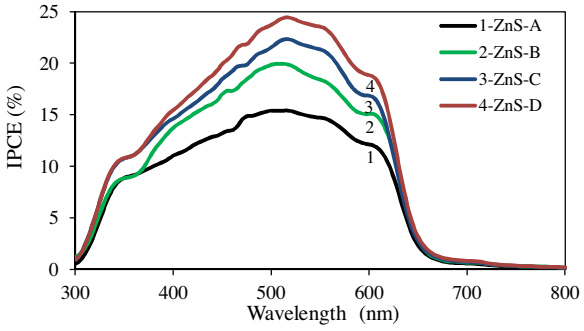


Fig. 8. IPCE spectra of the inverted devices using ZnS interlayer with different thicknesses.

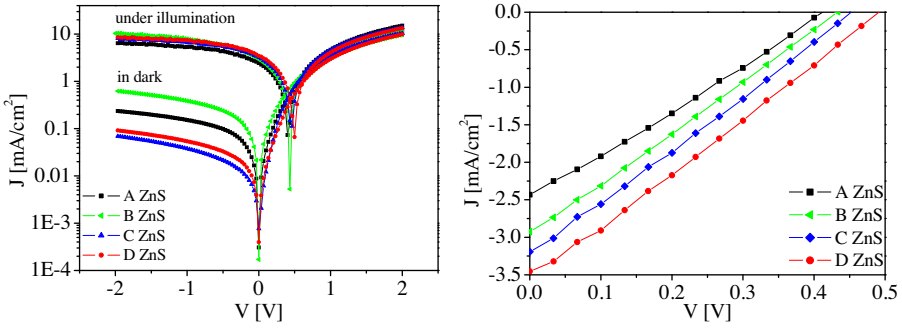


Fig. 6. Current density-voltage characteristics of the inverted devices using ZnS interlayer with different thicknesses, in dark and under simulated AM1.5 G illumination at 100 mW/cm^2.

The IPCE spectra of the inverted devices exhibited a broad range of response spanning from 300 to 650 nm and the intensity of spectra increased with relatively increasing optical transmittance due to decreasing thickness of ZnS interlayer. These results indicated that ZnS interlayer improved the charge collection and blocked the electrons at the active layer/ITO interference.

In an inverted geometry OPV, the low work function Al oxidized rapidly is replaced with more stable Ag or Au, which have higher work function, for eliminating the oxidation problem. The inverted geometry OPV is more stable and has a longer lifetime than the normal geometry OPV. The efficiency of inverted polymer solar cell decreases approximately linearly with time [41,42]. The stability and lifetime for the best device without encapsulation was measured in ambient conditions after 11 month. The photovoltaic performances of the device degraded as J_{sc} of 2.5 mA/cm^2, V_{oc} of 0.48 V, FF of 0.27 and PCE of 0.32%, compared to the initial photovoltaic performances. The power conversion efficiency of the inverted device designed with the thinnest ZnS interlayer decreased about 30% after 7920 h under ambient conditions.

4. Conclusion

In this study, inverted type hybrid solar cells in ITO/ZnS/P3HT:PCBM/PEDOT:PSS:IPA/Ag structure were fabricated. ZnS interlayer as an electron transport layer in this structure was deposited by the spray pyrolysis method at fixed substrate temperature. The optical and structural properties of the ZnS thin films annealed at different temperatures were examined in detail. The effects of annealing temperature and also thickness of ZnS interlayer on the efficiency of the devices were investigated. As the annealing temperatures for ZnS thin films were increased from 200 to 500 °C for 1 h, the efficiency of the devices significantly increased thanks to improvement of the electron transport and optical properties. XRD patterns and SEM images of ZnS interlayers showed that films with higher crystalline structure and smoother surface morphology were obtained as a result of increasing annealing temperature. Films, which are highly crystalline and having smooth surface, are important for the efficient charge transfer at the active layer/ITO interference. The power conversion efficiencies of the inverted devices with ZnS electron transport layers increased with decreasing thickness of ZnS interlayer annealed at 500 °C for 1 h. The best performance obtained in the inverted devices was about 0.45% when 135 nm of annealed ZnS thin film was used. The results indicated that photovoltaic performances of the inverted devices were found to be strongly dependent on annealing temperature and thickness of ZnS interlayer. The inverted organic solar cells based on ZnS interlayer exhibited remarkable long term stability.

Acknowledgement

This work was supported by Yıldız Technical University Scientific Research Project Coordination Department with project no 2015-01-01-DOP01.

References

[1] A.J. Heeger, 25th anniversary article: bulk heterojunction solar cells: understanding the mechanism of operation, Adv. Mater. 26 (2014) 10–28.
[2] M.C. Scharber, N.S. Sariciftci, Efficiency of bulk-heterojunction organic solar cells, Prog. Polym. Sci. 38 (2013) 1929–1940.
[3] S. Gunes, H. Neugebauer, N.S. Sariciftci, Conjugated polymer-Based organic solar cells, Chem. Rev. (2007) 1324–1338.
[4] N. Kaur, M. Singh, D. Pathak, T. Wagner, J.M. Nunzi, Organic materials for photovoltaic applications: review and mechanism, Synth. Met. 190 (2014) 20–26.
[5] G. Dennler, M.C. Scharber, C.J. Brabec, Polymer-fullerene bulk-heterojunction solar cells, Adv. Mater. 21 (2009) 1323–1338.
[6] J.D. Servaites, M.A. Ratner, T.J. Marks, Organic solar cells: a new look at traditional models, Energy Environ. Sci. 4 (2011) 4410.
[7] M. Girtan, On the stability of the electrical and photoelectrical properties of P3HT and P3HT:PCBM blends thin films, Org. Electron. Phys. Mater. Appl. 14 (2013) 200–205.
[8] K. Norrman, M.V. Madsen, S.A. Gevorgyan, F.C. Krebs, Degradation patterns in water and oxygen of an inverted polymer solar cell, J. Am. Chem. Soc. 132 (2010) 16883–16892.
[9] I. Litzov, C.J. Brabec, Development of efficient and stable inverted bulk heterojunction (BHJ) solar cells using different metal oxide interfaces, Materials 6 (2013) 5796–5820.
[10] T.M. Abdel-Fattah, E.M. Younes, G. Namkoong, E.M. El-Maghraby, A.H. Elsayed, A.H. Abo Elazm, Stability study of low and high band gap polymer and air stability of PTB7:PC71BM bulk heterojunction organic photovoltaic cells with encapsulation technique, Synth. Met. 209 (2015) 348–354.
[11] M. Jørgensen, K. Norrman, F.C. Krebs, Stability/degradation of polymer solar cells, Sol. Energy Mater. Sol. Cells. 92 (2008) 686–714.
[12] F. Ongul, Solution-processed inverted organic solar cell using V_2O_5 hole transport layer and vacuum free EGaIn anode, Opt. Mater. 50 (2015) 244–249.
[13] Y.E. Ha, M.Y. Jo, J. Park, Y.C. Kang, S.J. Moon, J.H. Kim, Effect of self-assembled monolayer treated ZnO as an electron transporting layer on the photovoltaic properties of inverted type polymer solar cells, Synth. Met. 187 (2014) 113–117.
[14] Y. Sun, J.H. Seo, C.J. Takacs, J. Seifter, A.J. Heeger, Inverted polymer solar cells integrated with a low-Temperature-Annealed sol-Gel-Derived ZnO film as an electron transport layer, Adv. Mater. 23 (2011) 1679–1683.
[15] S.K. Hau, H.-L. Yip, O. Acton, N.S. Baek, H. Ma, A.K.-Y. Jen, Interfacial modification to improve inverted polymer solar cells, J. Mater. Chem. 18 (2008) 5113.
[16] M. Wright, A. Uddin, Organic-inorganic hybrid solar cells: a comparative review, Sol. Energy Mater. Sol. Cells. 107 (2012) 87–111.
[17] J. Han, Z. Liu, K. Guo, J. Ya, Y. Zhao, X. Zhang, T. Hong, J. Liu, High-Efficiency $AgInS_2$-Modified ZnO nanotube array photoelectrodes for all-Solid-State hybrid solar cells, ACS Appl. Mater. Interfaces 6 (2014) 17119–17125.
[18] Z. Liu, J. Han, K. Guo, X. Zhang, T. Hong, Jalpaite Ag_3CuS_2: a novel promising ternary sulfide absorber material for solar cells, Chem. Commun. 51 (2015) 2597–2600.
[19] J. Han, Z. Liu, X. Zheng, K. Guo, X. Zhang, T. Hong, B. Wanga, J. Liua, Trilaminar ZnO/ZnS/Sb2S3 nanotube arrays for efficient inorganic?organic hybrid solar cells, RSC Adv. 4 (2014) 23807.
[20] N. Yavuz, S.A. Yuksel, A. Karsli, S. Gunes, Inverted structure hybrid solar cells using CdS thin films, Sol. Energy Mater. Sol. Cells 116 (2013) 224–230.
[21] S. Aydin Yuksel, S. Gunes, H.Y. Guney, Hybrid solar cells using CdS thin films deposited via spray pyrolysis technique, Thin Solid Films 540 (2013) 242–246.
[22] M. Bredol, K. Matras, A. Szatkowski, J. Sanetra, A. Prodi-Schwab, P3HT/ZnS: A new hybrid bulk heterojunction photovoltaic system with very high open circuit voltage, Sol. Energy Mater. Sol. Cells 93 (2009) 662–666.
[23] T. Kuwabara, M. Nakamoto, Y. Kawahara, T. Yamaguchi, K. Takahashi, Characterization of ZnS-layer-inserted bulk-heterojunction organic solar cells by ac impedance spectroscopy, J. Appl. Phys. 105 (2009) 124513.
[24] X. Wu, F. Lai, L. Lin, J. Lv, B. Zhuang, Q. Yan, et al., Applied Surface Science Optical inhomogeneity of ZnS films deposited by thermal evaporation, Appl. Surf. Sci. 254 (2008) 6455–6460.
[25] M.M. Islam, S. Ishizuka, A. Yamada, K. Sakurai, S. Niki, T. Sakurai, et al., CIGS solar cell with MBE-grown ZnS buffer layer, Sol. Energy Mater. Sol. Cells 93 (2009) 970–972.
[26] M.A. Ehsan, T.A.N. Peiris, K.G.U. Wijayantha, H. Khaledi, H.N. Ming, M. Misran, et al., Surface morphological and photoelectrochemical studies of ZnS thin films developed from single source precursors by aerosol assisted chemical vapour deposition, Thin Solid Films 540 (2013) 1–9.
[27] S.W. Shin, S.R. Kang, K.V. Gurav, J.H. Yun, J.-H. Moon, J.Y. Lee, et al., A study on the improved growth rate and morphology of chemically deposited ZnS thin film buffer layer for thin film solar cells in acidic medium, Sol. Energy 85 (2011) 2903–2911.
[28] M.C. López, J.P. Espinos, F. Martín, D. Leinen, J.R. Ramos-Barrado, Growth of ZnS thin films obtained by chemical spray pyrolysis: the influence of precursors, J. Cryst. Growth 285 (2005) 66–75.
[29] G.B. Williamson, R.C. Smallman, Dislocation densities in some annealed and cold worked metals from measurements on the X-ray Debye-Scherrer spectrum, Philos. Mag. 1 (1956) 34–46.
[30] Amorphous & Liquid Semiconductors, in: J. Tauc (Ed.), Plenum Press, New York, 1974, pp. 159.
[31] Y.N. Xu, W.Y. Ching, Electronic, optical, and structural properties of some wurtzite crystals, Phys. Rev. B 48 (1993) 4335–4351.
[32] M. Wildner, G. Giester, Crystal structure refinements of synthetic chalcocyanite ($CuSO_4$) and zincosite ($ZnSO_4$), Mineral. Petrol. 39 (1988) 201–209.
[33] K. Kihara, G. Donnay, Anharmonic thermal vibrations in ZnO, Can. Mineral. 23 (1985) 647–654.
[34] J. Díaz-Reyes, R.S. Castillo-Ojeda, R. Sanchez-Espíndola, M. Galvan-Arellano, O. Zaca-Moran, Structural and optical characterization of wurtzite type ZnS, Curr. Appl. Phys. 15 (2014) 103–109.
[35] J.S. McCloy, W. Wolf, E. Wimmer, B.J. Zelinski, Impact of hydrogen and oxygen defects on the lattice parameter of chemical vapor deposited zinc sulfide, J. Appl. Phys. 113 (2013).

[36] S.P. Patel, J.C. Pivin, V.V. Siva Kumar, A. Tripathi, D. Kanjilal, L. Kumar, Grain growth and structural transformation in ZnS nanocrystalline thin films, Vacuum 85 (2010) 307–311.
[37] C.A. Rodríguez, M.G. Sandoval-Paz, G. Cabello, M. Flores, H. Fernández, C. Carrasco, Characterization of ZnS thin films synthesized through a non-toxic precursors chemical bath, Mater. Res. Bull. 60 (2014) 313–321.
[38] Y. He, L. Zhang, L. Wang, M. Li, X. Shang, X. Liu, Y. Lu, B.K. Meyer, Structural and optical properties of single-phase $ZnO_{1-x}S_x$ alloy films epitaxially grown by pulsed laser deposition, J.Alloys Compd. 587 (2014) 369–373.
[39] M.H. Doha, M.J. Alam, J. Rabeya, K.A.M.H. Siddiquee, S. Hussain, O. Islam, M.A. Gafur, S. Islam, N. Khatun, S.H. Sarkard, Characterization of chemically deposited ZnS thin films on bare and conducting glass, Optik 126 (2015) 5194–5199.
[40] X. Ren, Zhou Yang, D. Yang, X. Zhang, D. Cui, Y. Liu, Q. Wei, H. Fan, S. Liu, Modulating crystal grain size and optoelectronic properties of perovskite film for solar cell application by reaction temperature, Nanoscale 8 (2016) 3816–3822.
[41] S.W. Heo, K.H. Baek, T.H. Lee, J.Y. Lee, D.K. Moon, Enhanced performance in inverted polymer solar cells via solution process: morphology controlling of PEDOT:PSS as anode buffer layer by adding surfactants, Mater. Appl. 14 (2013) 1629–1635.
[42] Y.J. Noh, S.I. Na, S.S. Kim, Inverted polymer solar cells including ZnO electron transport layer fabricated by facile spray pyrolysis, Sol. Energy Mater. Sol. Cells 117 (2013) 139–144.